Synthesis of High Surface Area, Water-Dispersible Graphitic Carbon Nanocages by an in Situ Template Approach

Jian Nong Wang,*,† Li Zhang,† Jun Jie Niu,† Fan Yu,† Zhao Ming Sheng,† Yu Zeng Zhao,† Hyuk Chang,‡ and Chanho Pak‡

School of Materials Science and Engineering, Shanghai Jiao Tong University, 1954 Huashan Road, Shanghai 200030, P.R. China, and Samsung Advanced Institute of Technology, P.O. Box 111, Suwon 440-600, Korea

Received October 18, 2006. Revised Manuscript Received November 28, 2006

This study reports an approach for synthesis of graphitic carbon nanocages (CNCs) via pyrolysis of ethanol with dissolved iron carbonyl at temperatures from 600 to 900 °C. The in situ formed Fe catalyst and template enabled the in situ generation of carbon from ethanol and formation of graphitic layers on the template surface. With the removal of the template, hollow CNCs were obtained to have a fine size of 30−50 nm and a large surface area of 400−800 m^2/g. The CNCs also became dispersible in water without aggregation and settling after several months through HNO_3 treatment. As an example for potential applications, the CNCs were demonstrated to be a good material for supporting the Pt catalyst used in low-temperature fuel cells. Considering its continuous and low-temperature operation, in situ formation of catalyst and template, and in situ graphitization of decomposed carbon, the present approach may be suitable for large-scale production of high surface area and water-dispersible graphitic carbon and would be practically relevant for many technologies.

1. Introduction

It is well-known that nanostructured carbon materials have wide applications in information technology, biochemistry, environment, and energy industries.[1] This has triggered many studies on the control of the structure, nature, and surface chemistry of nanoporous carbon to meet the requirements of specific applications. For the intended applications as adsorbents, catalyst supports, electrode materials, and energy storage media, a nanostructure with a high surface area is of particular importance, and graphitic carbon is advantageous over amorphous carbon because graphitic carbon has a well-developed crystalline structure, high electric conductivity, good thermal stability, and satisfactory oxidation resistance at low temperature.[2] For the applications in catalysis, development of artificial cells, delivery of drugs and dyes, and protection of biologically active agents, the nanoporous carbon should be populated on its surface by a functional secondary material, or at least dispersible or soluble in water, a medium essential to studies involving live cells.[3] Thus, the synthesis of high surface area, water-dispersible graphitic carbon materials is of great interest in the applications listed above.

Arc discharge, laser evaporation, and chemical vapor deposition[4] are the general techniques used for synthesizing graphitic carbon materials such as carbon nanotubes,[4a−c] hollow carbon nanocages (CNCs),[4d] solid carbon nanospheres,[4e−g] and carbon nanofibers.[4h] Most of the materials synthesized by these techniques exhibit a low surface area and low yield. Conventional activating agents such as H_2O and CO_2 fail to activate graphitic carbons, usually used to develop a high surface area. Severe activation, using alkali compounds as activating agent, such as KOH, can provide a high surface

* To whom correspondence should be addressed. Fax: +86-21 62932587. E-mail: jnwang@mail.sjtu.edu.cn.

† Shanghai Jiao Tong University.

‡ Samsung Advanced Institute of Technology.

(1) Marsh, H.; Heintz, E. A.; Rodriguez-Reinoso, F. *Introduction to Carbon Technology*; Universidad de Alicante, Secretariado de Publications: Alicante, Spain, 1997.

(2) (a) Ryoo, R.; Joo, S. H.; Jun, S. *J. Phys. Chem. B* **1999**, *103*, 7743. (b) Lu, A.-H.; Schmidt, W.; Spliethoff, B.; Schüth, F. *Adv. Mater.* **2003**, *15*, 1602. (c) Lu, A.-H.; Schmidt, W.; Matoussevitch, N.; Bönnermann, H.; Spliethoff, B.; Tesche, B.; Bill, E.; Kiefer, W.; Schüth, F. *Angew. Chem., Int. Ed.* **2004**, *43*, 4303. (d) Lee, J.; Han, S.; Hyeon, T. *J. Mater. Chem.* **2004**, *14*, 478. (e) El Hamaoui, B.; Zhi, L.; Wu, J.; Kolb, U.; Müllen, K. *Adv. Mater.* **2005**, *17*, 2957.

(3) (a) Zhong, Z.; Yin, Y.; Gates, B.; Xia, Y. *Adv. Mater.* **2000**, *12*, 206. (b) Liang, H. P.; Zhang, H. M.; Hu, J. S.; Guo, Y. G.; Wan, L. J.; Bai, C. L. *Angew. Chem., Int. Ed.* **2004**, *43*, 1540. (c) Hu, Y.; Chen, J. F.; Chen, W. M.; Li, X. L. *Adv. Funct. Mater.* **2004**, *14*, 383. (d) Lytle, J. C.; Yan, H.; Ergang, N. S.; Smyrl, W. H.; Stein, A. *J. Mater. Chem.* **2004**, *14*, 1616. (e) Yoon, S. B.; Chai, G. S.; Kang, S. K.; Yu, T. S.; Gierszal, K. P.; Jaroniec, M. *J. Am. Chem. Soc.* **2005**, *127*, 4188. (f) Liang, F.; Beach, J. M.; Rai, P. K.; Guo, W.; Hauge, R. H.; Pasquali, M.; Smalley, R. E.; Billups, W. E. *Chem. Mater.* **2006**, *18*, 1520.

(4) (a) Journet, C.; Master, W. K.; Bernier, P.; Loiseau, A.; Lamy de la Chapellw, M.; Lefrant, S.; Deniard, P.; Lee, R.; Fisher, J. E. *Nature* **1997**, *388*, 756. (b) Thess, A.; Lee, R.; Nikolaev, P.; Dai, H. J.; Petit, P.; Robert, J.; Xu, C. H.; Lee, Y. H.; Kim, S. G.; Rinzler, A. G.; Colbert, D. T.; Scuseria, G. E.; Tomanek, D.; Fisher, J. E.; Smalley, R. E. *Science* **1996**, *273*, 483. (c) Terrones, M.; Grobert, N.; Olivares, J.; Zhang, J. P.; Terrones, H.; Kordatos, K.; Hsu, W. K.; Hare, J. P.; Townsend, P. D.; Prassides, K.; Cheetham, A. K.; Kroto, H. W.; Walton, D. R. M. *Nature* **1997**, *388*, 52. (d) Saito, Y.; Matsumoto, T. *Nature* **1998**, *392*, 237. (e) Choi, M.; Altman, I. S.; Kim, Y.-J.; Pikhitsa, P. V.; Lee, S.; Park, G.-S.; Jeong, T.; Yoo, J.-B. *Adv. Mater.* **2004**, *16*, 1721. (f) Liu, X. Y.; Huang, B. C.; Coville, N. J. *Carbon* **2002**, *40*, 2791. (g) Qiao, W. M.; Song, Y.; Lim, S. Y.; Hong, S. H.; Yoon, S. H.; Mochida, I.; Imaoka, T. *Carbon* **2006**, *44*, 158. (h) Yoon, S. H.; Lim, S. Y.; Hong, S. H.; Qiao, W. M.; Whitehurst, D. D.; Mochida, I.; An, B.; Yokogawa, K. *Carbon* **2005**, *43*, 1828.

10.1021/cm062491d CCC: $37.00
Published on Web 01/13/2007

area, but result in a remarkable degradation of the graphitic structure and substantial material loss.[5]

Heat treatment of porous carbon at temperatures higher than 2000 °C is able to form well-developed graphitic structures. But this normally leads to a significant reduction in surface area and pore volume.[6] To overcome such deficiencies, several methods were developed in recent years. They basically involved the use of a transition metal to catalyze the graphitization of amorphous carbons at lower temperatures (~1000 °C). Depending on the starting materials and experimental conditions used, different graphitic carbons were prepared, such as graphitic nanoribbons,[7] ordered graphitic domains,[8] graphitic nanocoils or nanocages,[9] and graphitic porous carbon.[10] Nevertheless, the preparation of each of these materials includes preparation of carbon precursors (e.g., aerogel or polymer particles) and mixing of the precursors with catalytic particles and thus suffers from time-consuming, incomplete graphitization, difficult purification of remaining amorphous carbon, and low surface areas (~300 m^2/g).

Recently, a template method was demonstrated and appears promising. That is, fine polymeric or inorganic particles were used as the template for the formation of carbon layers on their surfaces. From such particles with a core−shell structure, hollow CNCs were obtained by removing the template at the core.[11] Graphitized nanoporous carbons with surface areas of 240−460 m^2/g were prepared by heat treatment over 2400 °C of the pitch-based mesoporous carbons obtained by using silica colloidal crystal and nanosilica as templates.[12] Ordered mesoporous carbon with graphitic framework structures was synthesized through in situ conversion of an aromatic compound, acenaphthene, to mesophase pitch inside the silica templates.[13] However, these reported template methods usually require the synthesis of the template first, then mixing of the template with the carbon source material, and finally graphitization of the carbon. Thus, multiple steps are involved, leading to a complicated procedure.

The synthetic processes discussed above either require high temperatures or are rather time-consuming, and in most cases give rise to relatively low surface areas. Therefore, up to now, it is still a great challenge to find a simple method suitable for large-scale production of graphitic porous carbon with high surface area. In the present study, a novel template method is reported, in which both the template of Fe particles and the shell of graphitic layers can be formed through one-step pyrolysis of ethanol containing iron pentacarbonyl. Further, the resultant graphitic CNCs are acid-treated to remove the in situ template or catalyst to finally prepare hollow CNCs with high dispersion in water and high surface area.

2. Experimental Section

2.1. Synthetic Procedure. In the present study, a quartz tube with an inner diameter of 30 mm and a length of 1500 mm was used as the reactor for pyrolysis and placed vertically in an electrical furnace with a heating length of 600 mm. Liquid iron pentacarbonyl [$Fe(CO)_5$] was dissolved in ethanol with a volume ratio of 1:5. The resulting solution was supplied at a rate of 60 mL/h and carried into the reactor by nitrogen with a flow rate of 80 L/h. The furnace temperature was set at 600, 750, and 900 °C and the as-prepared sample was collected at the bottom of the quartz tube. To remove the Fe particles, the as-prepared sample was refluxed in HCl or HNO_3 at 100 °C for 2 h. This was followed by washing with distilled water several times and drying at 80 °C for 3 h. To investigate the dispersion of the CNCs in water, different amounts of CNCs after nitric acid treatment were ultrasonicated in water to have concentrations from 0.0155 to 0.124 g/L.

2.2. Characterization. X-ray diffraction (XRD) experiments were conducted on specimens before and after template removal. The X-ray diffractometer (Bruker D8 Advance, Bruker AXS, Germany) was operated at 40 kV and 40 mA. Nickel-filtered Cu Kα radiation was used in the incident beam. High-resolution electron transmission microscopy (HRTEM) with a cold field emission gun (Jeol-2010F) was used to study the microstructure and morphology of the as-prepared and purified samples. The samples were dispersed in ethanol by means of a sonicator and scooped up with a holey amorphous carbon film for TEM observations. Fourier transform infrared (FT-IR) spectra of as-prepared and as-purified carbons were collected on an EQUNOX 55 FT-IR spectrometer from 4000 to 400 cm^{-1}.

Nitrogen (at 77 K) adsorption isotherm of CNC was measured using a BELSORP instrument (BEL, Japan, Inc.). The sample was outgassed at 200 °C under nitrogen flow for 4 h prior to the measurement. Total surface area of CNC was calculated according to the BET equation from the adsorption data in the relative pressure from 0.04 to 0.2. Finally, pore volumes were estimated to be the liquid volume of adsorption (N_2) at a relative pressure of 0.99. The micropore size distribution (<2 nm) was determined by micropore analysis method (MP method), derived from the curvature of the t-plot which was calculated from N_2 adsorption isotherm. And the mesopore size distribution (>2 nm) was determined by the Barrett−Joyner−Halenda (BJH) method. Details about these analytical methods can be found in ref 14.

2.3. Deposition of Pt and Measurement of Electrochemical Activity. *Preparation of Pt/Carbon Catalysts.* Two kinds of catalyst were prepared with two different supports, the present carbon

(5) (a) Delpeux, S.; Szostak, K.; Frackowiak, E.; Beguin, F. *Chem. Phys. Lett.* **2005**, *404*, 374. (b) Lee, S. M.; Lee, S. C.; Jung, J. H.; Kim, H. J. *Chem. Phys. Lett.* **2005**, *416*, 251. (c) Raymundo-Pinero, E.; Azais, P.; Cacciaguerra, T.; Cazorla-Amoros, D.; Linares-Solano, A.; Beguin, F. *Carbon* **2005**, *43*, 786. (d) Yoon, S. H.; Lim, S. Y.; Song, Y.; Yasunori, O.; Qiao, W. M.; Atsushi, T.; Mochida, I. *Carbon* **2004**, *42*, 1723. (e) Mitani, S.; Lee, S. I.; Yoon, S. H.; Korai, Y.; Mochida, I. *J. Power Sources* **2004**, *133*, 298. (f) Qiao, W. M.; Yoon, S. H.; Mochida, I. *Energy Fuels* **2006**, *20*, 1680.
(6) Hanzawa, Y.; Hatori, H.; Yoshizawa, N.; Yamada, Y. *Carbon* **2002**, *40*, 575.
(7) Fu, R.; Baumann, T. F.; Cronin, S.; Dresselhaus, G.; Dresselhaus, M. S.; Satcher, J. H., Jr. *Langmuir* **2005**, *21*, 2647.
(8) Maldonado-Hodar, F. J.; Moreno-Castilla, C.; Rivera-Utrilla, J.; Hanzawa, Y.; Yamada, Y. *Langmuir* **2000**, *16*, 4367.
(9) (a) Hyeon, T.; Han, S.; Sung, Y.-E.; Park, K.-W.; Kim, Y.-W. *Angew. Chem., Int. Ed.* **2003**, *42*, 4352.(b) Han, S. J.; Yun, Y.; Park, K. W.; Sun, Y. E.; Hyeon, T. *Adv. Mater.* **2003**, *15*, 1922.
(10) (a) Lu, A.-H.; Li, W.; Matoussevitch, N.; Spliethoff, B.; Bönnemann, H.; Schüth, F. *Chem. Commun.* **2005**, *1*, 98. (b) Lu, A.-H.; Li, W.-C.; Salabas, E.-L.; Spliethoff, B.; Schüth, F. *Chem. Mater.* **2006**, *18*, 2086.
(11) (a) Tamai, H.; Sumi, T.; Yasuda, H. *J. Colloid Interface Sci.* **1996**, *177*, 325. (b) Yoon, S. B.; Sohn, K.; Kim, J. Y.; Shin, C. H.; Yu, J. S. *Adv. Mater.* **2002**, *14*, 19.
(12) (a) Yoon, S. B.; Chai, G. S.; Kang, S. K.; Yu, J.-S.; Gierszal, K. P.; Jaroniec, M. *J. Am. Chem. Soc.* **2005**, *127*, 4188. (b) Qiao, W. M.; Song, Y.; Hong, S. H.; Lim, S. Y.; Yoon, S. H.; Korai, Y.; Mochida, I. *Langmuir* **2006**, *22*, 3791.
(13) Kim, T.-W.; Park, I.-S.; Ryoo, R. *Angew. Chem., Int. Ed.* **2003**, *42*, 4375.

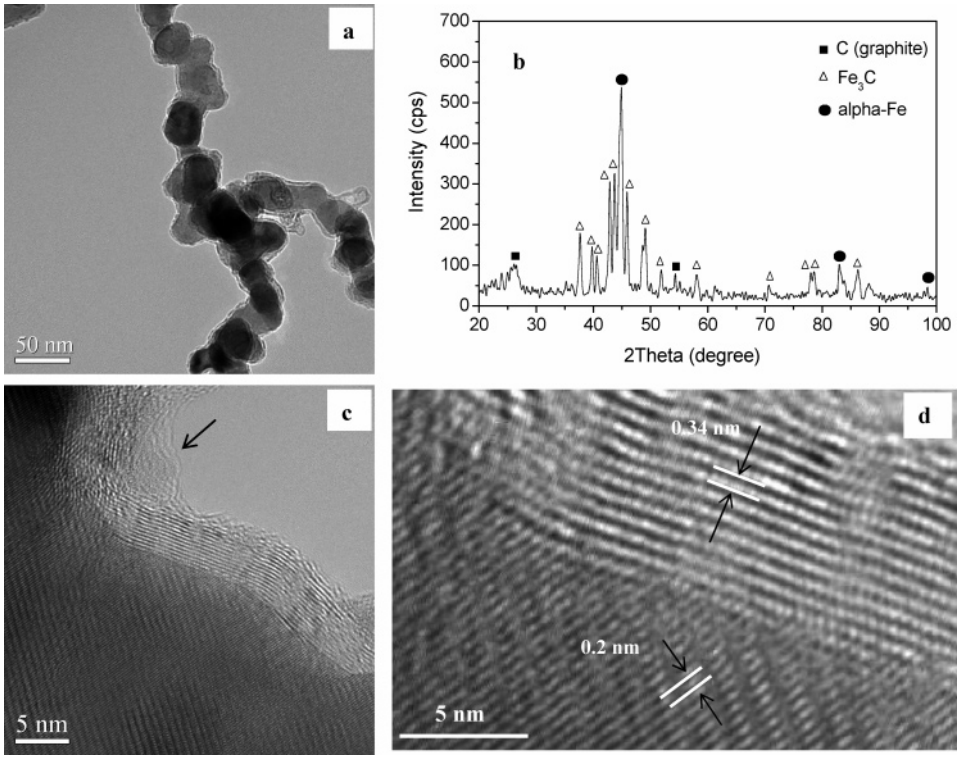

Figure 1. TEM image (a), XRD pattern (b), and HRTEM image (c, d) of the sample synthesized at 700 °C, showing the core−shell structure and phase constitution. Minor amorphous carbon on particle surface is arrowed in (c).

nanocages (Pt/CNC) and the conventional carbon black (Vulcan XC72) (Pt/CB). In each case, the carbon slurry was prepared by mixing carbon vigorously with the distilled water. Then the slurry was heated up to a desired temperature around 90 °C. The pH of the slurry was adjusted to the basic using $NaHCO_3$. The chloroplatinic acid (CPA) solution, prepared by dissolving CPA (H_2PtCl_6) into the distilled water, was added to the carbon slurry and the pH of the slurry was again adjusted to the basic. The reducing agent of ethanol was then introduced into the slurry for in situ liquid-phase reduction. The Pt/carbon slurry was filtered, washed, and then dried at 80 °C in vacuum. The Pt loading was controlled to be 45% (weight percentage).

Cyclic Voltammetry. The electrochemical activities of the two catalysts (Pt/CNC, Pt/CB) were characterized by cyclic voltammetry (CV) technique. The experiments were performed using a three-electrode cell using an EG&G potentiostat (Model 366A) at ambient temperature. A saturated calomel electrode (SCE) and a large area Pt plate were used as the reference electrode and counter electrode, respectively, and 0.5 M H_2SO_4 was used as electrolyte. The CV profiles were recorded at a scan rate of 100 mV/s from the potential of −0.241 to 0.959 V vs SCE. For comparison, a commercial catalyst from John Mathney was also used and studied under otherwise identical conditions.

3. Results

3.1. Structure of CNC Samples with Template. Experiments showed that when only ethanol was injected into the high-temperature zone, the ethanol evaporated at the upper part of the furnace was condensed back to liquid at the lower part of the furnace. This indicates that the decomposition of ethanol was limited with almost no carbon product produced. However, when ethanol was added with iron carbonyl, black powder was continuously produced, but with some liquid ethanol still remaining in the gas stream. Rough estimation revealed that the amount of sample produced per hour increased with increasing temperature from 600 to 900 °C. Under the present experimental conditions (typically, reactor diameter, ∼3 cm; supply rate of spray solution, 60 mL/h; and temperature, 700 °C), the production rate of the sample was about 10 g/h.

A typical TEM image of the sample prepared at 700 °C is shown in Figure 1a. As can be seen, the sample consisted of nanoparticles with an average diameter of 30−50 nm. Furthermore, each nanoparticle had a core−shell structure with the core containing Fe and the shell being carbon. The XRD pattern is illustrated in Figure 1b. The peaks at $2\theta = 26.22°$ and 54.34° can be attributed to the diffractions of the (002) and (004) planes of the hexagonal structure of graphite. Those appearing at $2\theta = 44.9°$, 82.9°, and 98° result from the diffractions of (110), (211), and (220) planes of α-Fe, and the rest of the peaks are related to the Fe_3C phase. HRTEM (Figure 1c) revealed an ordered crystalline structure both in the shell and in the core. Since the interlayer spacing of the lattice fringes in the shell is about 0.34 nm (Figure 1d), the imaged lattice plane is the (002) plane of graphite. Since the interlayer spacing of the lattice fringes in the core is about 0.2 nm (Figure 1d), the imaged lattice is the (102) plane of Fe_3C.

The samples prepared at 600 and 900 °C are similar to that prepared at 700 °C. That is, all particles contained a metallic core and a graphitic shell. Except for such particles, other impurities such as carbon nanotubes or nanofibers were rarely observed. A minor amount of amorphous carbon was

(14) (a) Myers, D. *Surfaces, Interfaces, and Colloids: Principles and Applications*; Wiley-VCH: NewYork, 1999. (b) Gregg, S. J.; Sing, K. S. W. *Adsorption, Surface Area, and Porosity*; Academic Press: New York, 1982. (c) Lippens, B. C.; De Boer, J. H. *J. Catal.* **1965**, *4*, 319.

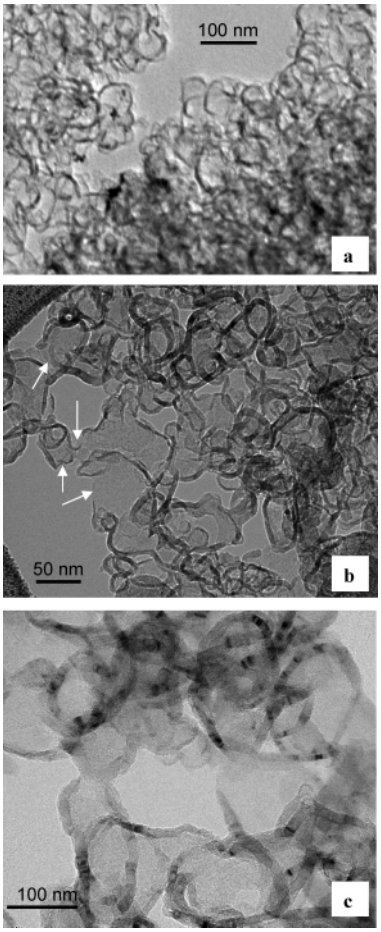

Figure 2. TEM images of hollow carbon nanocages from samples synthesized at 600 (a), 700 (b), and 900 °C (c), showing the differences in cage size and shell thickness between the lower temperature samples and the higher temperature one. Cage opening is arrowed in (b).

found only on the surface of the nanoparticle as seen in Figure 1c. However, as the temperature was increased to 900 °C, the size of the nanoparticles became larger than 100 nm, and the thickness of the graphitic shell larger than 10 nm.

3.2. Structure of CNC Samples without Template. The change in particle size with temperature can be better seen after the sample is purified with acid. As shown in Figure 3, the original Fe or Fe_3C phase vanished but carbon shells remained with their sizes varying with temperature from 600 to 900 °C. HRTEM (Figure 4) illustrates that the shell was still constituted by graphitic layers with a spacing of 0.34 nm. The removal of core materials and remainder of graphitic shells can be further supported by XRD results. Compared with the as-prepared sample, the purified one shows no strong peaks of Fe but a strong peak of graphite at $2\theta = 26.22°$. The weak peak seen at $2\theta = \sim 43°$ may be assigned to Fe_3C ((102) plane). This observation suggests that some Fe_3C phase remained in the final samples.

CNCs become hollow after acid treatment as shown in Figures 2 and 3. This suggestion is supported by the observations of the lack of structure and uniform translucent appearance to the electron beam in the core region (Figure 3), and similar structures of graphitic planes in multiple overlaid particles (Figure 3b). If the cagelike particles were filled with amorphous carbon, then the interiors would show

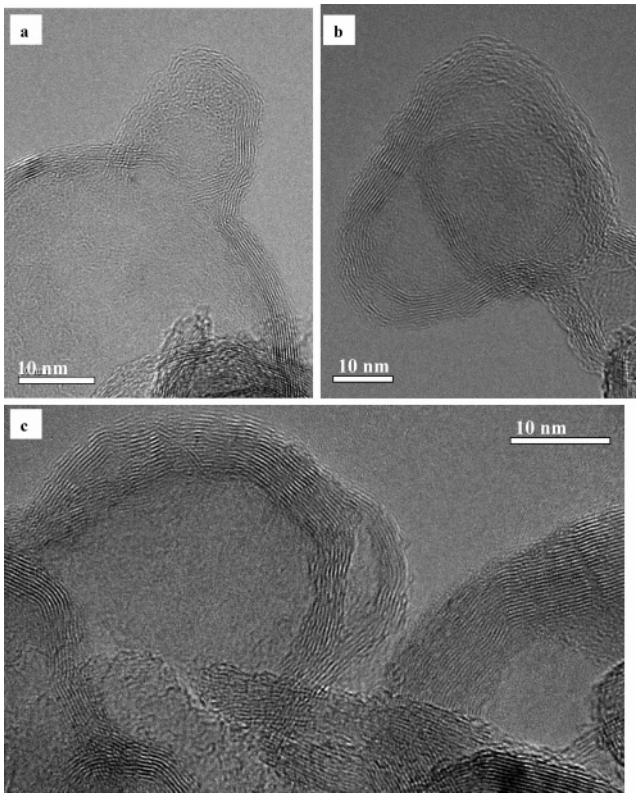

Figure 3. HRTEM images of hollow CNCs synthesized at 700 °C, showing graphitic layers in shells. Note the overlaid cages in (b).

variations of translucence and the structures behind the overlaid cages could not be clearly discerned. This is due to the intervening crystalline material in the path of the electron beam.

3.3. Porosity of Hollow CNCs. Several N_2 adsorption experiments were carried out to analyze the pore structures in the hollow cage samples synthesized at different temperatures. In Figure 5a, the N_2 adsorption isotherms show an uptake of N_2 in the region of low nitrogen pressure ($p/p_0 < 0.05$). This observation suggests that there were micropores in all cage samples. After the initial adsorption, however, the uptake of N_2 increased significantly in the region of high nitrogen pressure ($p/p_0 > 0.05$). Such a high uptake indicates the presence of mesopores in the samples.

With use of these adsorption data, the apparent specific surface area S_{BET} and the contributions of micropores and mesopores can be calculated based on the BET and BJH methods, respectively. Results (Table 1) show that the hollow CNCs synthesized at 600, 700, and 900 °C had a S_{BET} of 800, 433, and 201 m^2/g, respectively. Furthermore, almost all the surface areas were contributed by mesopores, and the contributions by micropores were very small.

Figure 5b shows the mesopore size distribution. A large number of mesopores ranging from 2 to 100 nm in size formed in the samples. Additionally, there were more such pores in the sample synthesized at a lower temperature than that synthesized at a higher temperature. Specifically, the samples synthesized at 600 and 700 °C present a strong distribution at pore sizes around 25 and 25−40 nm, respectively. These sizes are close to the inner diameters of the cages observed by TEM (Figure 2). Therefore, the pores of these sizes may result from the removal of the template

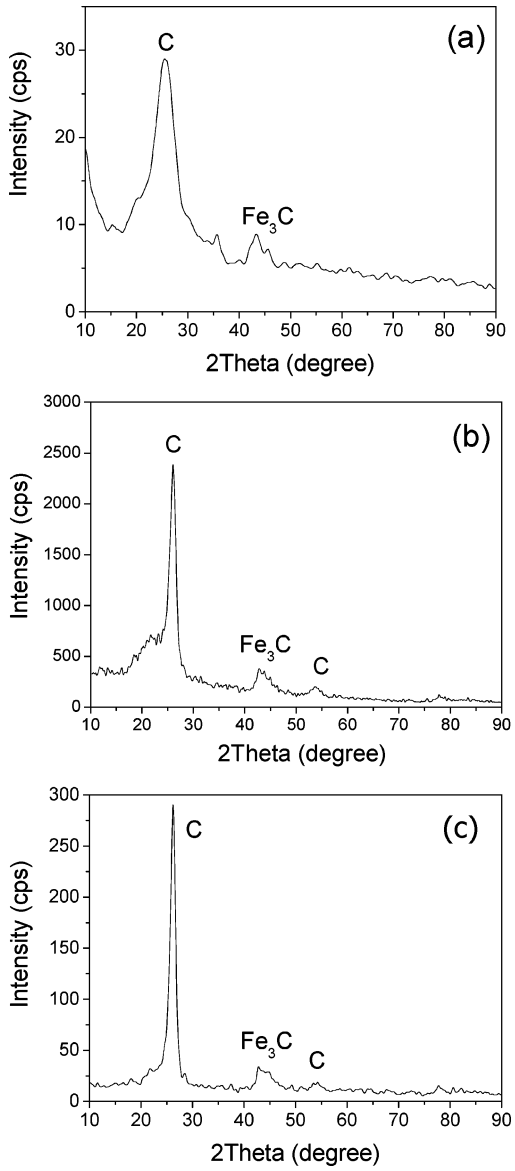

Figure 4. XRD patterns of hollow CNC samples synthesized at 600 (a), 700 (b), and 900 °C (c), showing evident reflections of graphite and remaining Fe_3C.

inside the cages and respond for the high S_{BET} values observed for the samples synthesized at 600 and 700 °C. Figure 5c illustrates the micropore size distributions. The results demonstrate that the micropores had dominant sizes ranging from 0.7 to 1.5 nm in all samples. Such pores may be produced by the acid treatment for removal of the template material.

3.4. Functionalization of Hollow CNCs. FT-IR spectroscopy was used to detect the development of the surface functional groups of graphitic carbon during nitric acid treatment, and the corresponding FT-IR spectra of carbons before and after this acid treatment are shown in Figure 6. After acid oxidation, one can see remarkable changes in the spectra as compared to the original one. Several new bands are present at 3419, 1720, 1581, and 1186 cm^{-1}. The band around 3419 cm^{-1} is attributed to the −OH or COOH groups in the graphitic carbon. FT-IR peaks appearing around 1720 and 1581 cm^{-1} can be assigned to the C═O stretching vibrations from ketones or carboxyl groups, although the 1581 cm^{-1} peak can also be ascribed to benzene C−C. The

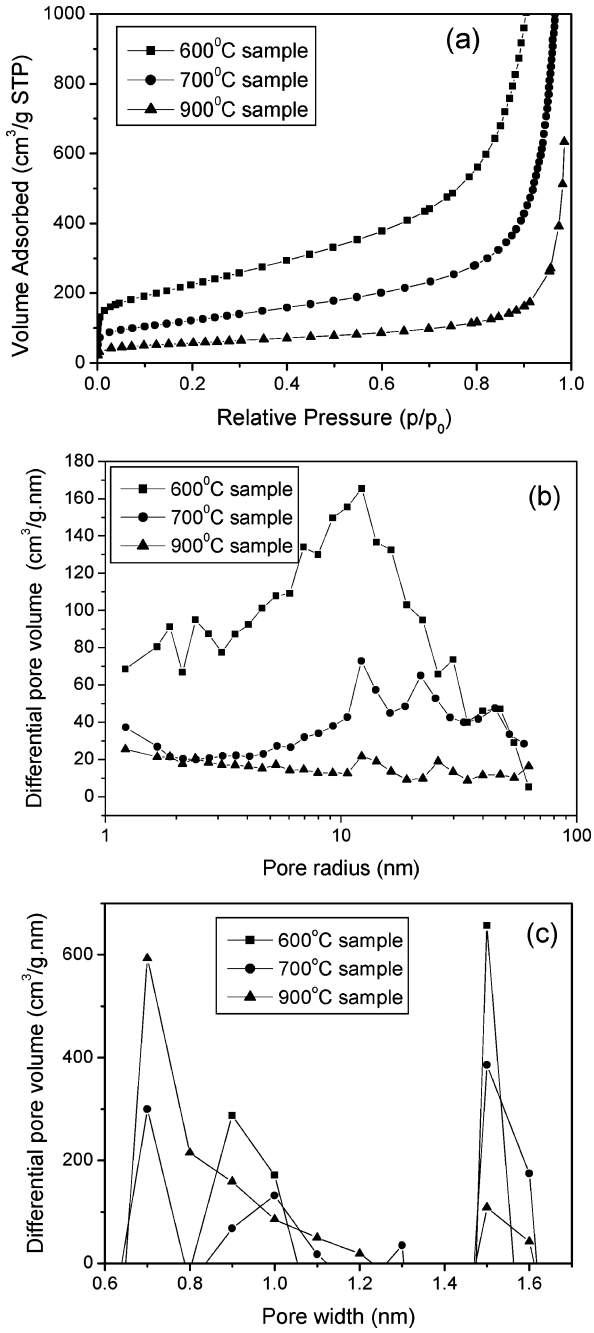

Figure 5. N_2 adsorption isotherms (a), mesopore size distributions (b), and micropore size distributions (c) of the samples synthesized at different temperatures. Note that, in Figure 5c, some lines contain only one or two data. Such lines are actually drawn based on more data which have differential volume values less than zero.

Table 1. Apparent Specific Surface Areas (S_{BET}) and Pore Volumes (V_{BET}) Measured by the BET Method and Contributions of Mesopores and Micropores Determined by the BJH Method for CNC Samples Synthesized at Different Temperatures after Template Removal

	600 °C	700 °C	900 °C
total S_{BET} (m^2/g)	800	433	201
$S_{mesopore}$ (m^2/g)	772	389	143
$S_{micropore}$ (m^2/g)	28	44	58
total V_{BET} (m^3/g)	4.47	0.91	1.37
$V_{macropore}$ (>50 nm)	1.66	0.02	0.82
$V_{mesopore}$ (2−50 nm)	2.73	0.86	0.5
$V_{micropore}$ (<2 nm)	0.08	0.03	0.05

band at 1186 cm^{-1} can be assigned to C−O−C vibrations in ether structures. These results provide clear evidence that

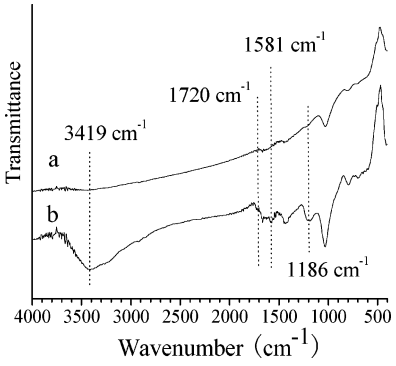

Figure 6. Infrared spectra of the samples before (a) and after (b) nitric acid treatment. Note the occurrence of new bands on (b).

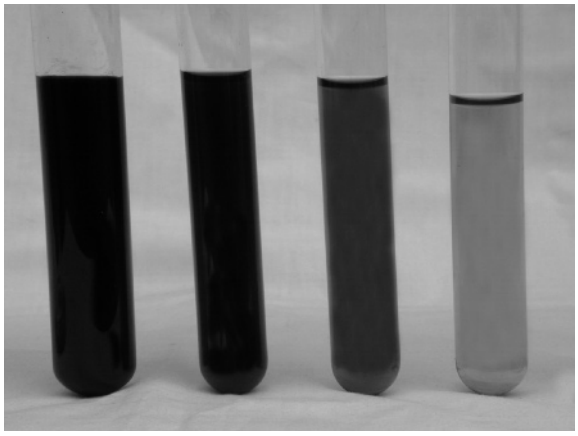

Figure 7. Water solutions containing different concentrations of carbon nanocages. From left to right: 0.124, 0.062, 0.031, and 0.0155 g/L, respectively. Note no indication of aggregation and settling after several months.

functional groups were successfully introduced, presumably on the external surface of the graphitic carbon, during the nitric acid treatment. However, it should be noted that the carbonyl bands associated with the carboxylic acid groups are weak. This may be a result of a combination of a low degree of functionalization and a relatively large spectral background in the low wavenumber region.

3.5. Dispersion of Hollow CNCs in Water. Figure 7 shows the dispersion of the CNCs in water. It was found that thermodynamically stable solutions were formed after sonication for 2 min. Visual inspection of these solutions revealed no indication of aggregation and settling of CNCs after several months. In contrast, a solution of the CNCs without nitric acid treatment began to show aggregation and settling within 2 min after sonication for 10 min.

3.6. Application as a Catalyst Support. To investigate the performance of the present hollow CNCs as a catalyst support for proton exchange membrane fuel cell electrodes, the sample originally synthesized at 700 °C was taken as an example, and an electrochemical study of a Pt catalyst (45 wt %) supported on this material (Pt/CNC) was conducted. For comparison, the same amount of Pt was also deposited on the conventional carbon black (Vulcan XC72) (Pt/CB). Platinum was generally uniformly dispersed on carbon black (Figure 8a) and CNCs (Figure 8b). Statistic estimation revealed that the average sizes of Pt particles on the two supports were ~5.0 and ~3.0 nm, respectively. These values are in close agreement with those estimated by the Scherrer's formula based on the XRD data shown in Figure 8c. Figure 8d shows the cyclic voltamograms of these two catalysts. The commercial catalyst from John Mathney Co. is also included for comparison. As can be seen, the catalyst of Pt/CNC demonstrates a stronger hydrogen adsorption peak and thus a higher activity than the catalyst of Pt/CB and the commercial catalyst as well.

4. Discussion

The present results expressly reveal the morphology and the structure of the CNCs filled with the Fe or Fe_3C template. The formation of this core−shell structure may be related to the activities of the carbon source and metal particles. The decomposition of $Fe(CO)_5$ might yield iron nanoparticles that possessed a very high catalytic activity for the decomposition of ethanol. At high temperature, the decomposed carbon could be dissolved in iron and form an Fe−C phase. As the temperature of the particles decreased, carbon would become oversaturated and would thus precipitate and deposit on the surface of the iron particles. Consequently, graphitic layers formed. With the removal of iron particles, hollow graphitic CNCs were obtained.

The large improvement in electrochemical activity from the catalyst of Pt/CB to that of Pt/CNC may be attributed to two factors. First, the Pt particles supported on CNCs exhibited a smaller size than those supported on Vulcan XC-72 CB (3.0 nm vs 4.5 nm) (Figures 8a and 8b). This difference could be related to the difference in specific surface area between the two supports (433 m^2/g vs 267 m^2/g). Second, the Pt particles supported on CNCs which had a graphitic structure may have a better electrical conductivity than those supported on the amorphous carbon black of Vulcan XC-72.

Several important features of the present graphitic carbon and synthesis process should be mentioned. First, the carbon precursor of ethanol was mixed with iron carbonyl at the molecular scale. Carbon was produced in situ from the decomposition of ethanol catalyzed by Fe particles. Consequently, the previous time-consuming preparation of carbon precursors (aerogel, R−F gel, or polymer particles) and mixing of the precursors with catalytic particles[7−10] were not needed. A further advantage of catalyzed decomposition of ethanol is that the generated carbon was dissolved in Fe particles and then precipitated out as graphitic layers. As a result, the as-prepared sample was of high purity, and previous impurities such as amorphous carbon[7−10] were rarely observed (Figure 1a).

Second, the Fe particles acted as a template for precipitation of carbon shell. Both the formation of this template and precipitation of graphitic layers took place in situ during the experiment, and thus previous separate procedures for preparing the template and additional steps for graphitization[11−13] were not required. Furthermore, since the whole process took place in short time, the size of the template was small, and the amount of carbon dissolved in the template was limited. All these led to particles of small size (<50 nm) and thin (<5 nm) and open graphitic shells (Figures 2a and 2b), and therefore high surface areas of 433 m^2/g at 700 and 800 m^2/g at 600 °C (Table 1). These values are much higher than

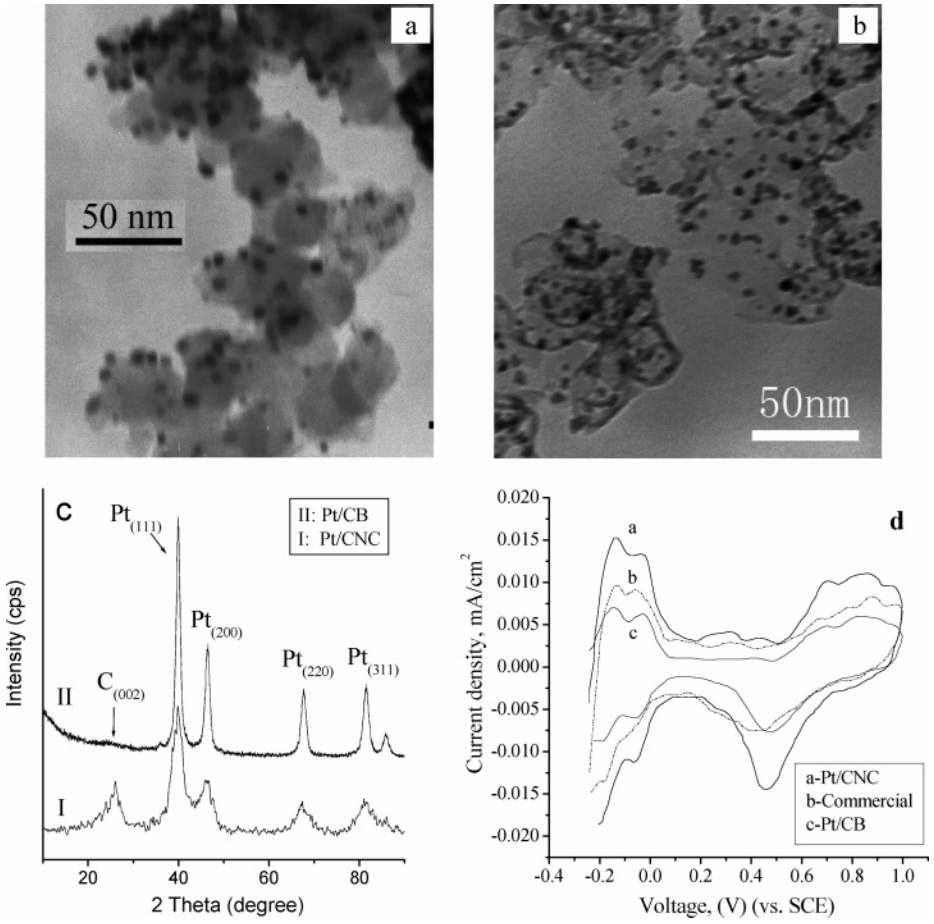

Figure 8. TEM images of the Pt/CB (a) and Pt/CNC (b) catalysts, their XRD patterns (c), and their cyclic voltamograms. Note the absence of a graphite peak for the Pt/CB catalyst but the presence of this peak for the Pt/CNC catalyst. A commercial catalyst from John Mathney Co. is included in (c) for comparison.

previous ones (generally up to 300 m^2/g) for graphitic carbon except for the mesoporous carbon[12b] with a surface area of 460 m^2/g but obtained at 2400 °C. The low surface area of 201 m^2/g for the present sample obtained at 900 °C may result from the CNCs having a large size (>100 nm) and a thick shell (~10 nm).

Third, in addition to high surface area and well-developed graphitic structure, the present CNCs also show good dispersion in water if they are treated in nitric acid (Figure 7). The reason for this observation may be that when hydrophilic functional groups (e.g., −OH, −COOH, C═O) are introduced on the surface, there will be an attractive interaction between water molecules and the nanocages. Hence, this mixture will be stable, and agglomeration and settling will not take place. However, the nanocage surface is hydrophobic without functional groups, and therefore there will be repulsive interaction between water molecules and the nanocages. Thus, this mixture will not be stable, and agglomeration and settling will take place.

Finally, the present synthesis process is continuous at low temperature and contains no harsh conditions. This is apparently advantageous over previous approaches by which samples could be produced only batch by batch. If the easy removal of the template and the high purity of the as-prepared material are taken into account, it becomes evident that the present approach may be suitable for large-scale production.

5. Conclusions

High surface area graphitic CNCs have been synthesized by pyrolysis of ethanol with dissolved iron carbonyl at low temperatures from 600 to 900 °C. Fe particles play important roles in in situ formation of template, carbon, and graphitic structure. With the removal of the Fe template, hollow CNCs are produced having a high purity, a fine size (30−50 nm), and a large surface area (400−800 m^2/g). When nitric acid is used for template removal, the hollow CNCs become dispersible in water without aggregation and settling after several months. When the CNCs were used as a catalyst support material, the electrochemical activity of the catalyst was apparently higher than the commercial catalyst and the catalyst using conventional carbon black as the support material. The present simple approach may be suitable for large-scale production of high surface area and water-dispersible graphitic carbon and would prove to be practically relevant for fuel cell technology.

Acknowledgment. We are thankful for support by The National Natural Science Foundation of China and Samsung Advanced Institute of Technology.

CM062491D